# Analysis of White LED Spectrum Based on CIE Color Spaces

Ziyao Xiong 02225789

***Abstract*---This report provides an analysis of a white LED's spectrum, obtained using a Michelson Interferometer with a He-Ne Laser reference for spectral accuracy. It includes an overview of white LED lighting principles and the methodology for extracting their XYZ components (red, green, blue) using CIE 1931 color spaces. This enables the quantification of key white light quality indicators: Correlated Color Temperature (CCT) and Color Rendering Index (CRI).**

## I. Introduction

THIS study utilizes the Michelson Interferometer, a pivotal instrument in optical physics developed by Albert A. Michelson in the late 19th century [1], to analyze the spectrum of white light emitted by LEDs. Operating on the principle of interference, the Michelson Interferometer is renowned for its precision in measuring minuscule distances, facilitating a detailed exploration of the LED spectrum.

Light Emitting Diodes (LEDs) represent a technological breakthrough in lighting, offering advantages such as efficacy, longevity, and compactness over traditional lighting solutions [2]. However, their adoption for consumer lighting has been met with some resistance, largely due to perceptions regarding the 'harshness' of light from white LED fixtures compared to the 'warmth' of incandescent bulbs [3].

Our research seeks to unravel the underlying reasons for this perceived disparity. We employed the International Commission on Illumination (CIE) color matching functions to extract XYZ components from white LED light, thereby assessing its color properties. The CIE functions provide quantitative connections between the visible spectrum's wavelength distributions and colors perceived by human vision [4]. Additionally, we compared the spectrum of white LED light with sunlight, calculating Correlated Color Temperature (CCT) and Color Rendering Index (CRI) to quantify variations in color rendition and quality.

## II. Theory

### A. Interferometer, interferogram, and spectrum

In the Michelson interferometer as shown in Figure 1, light splits into two beams with distinct paths. These beams recombine, creating interference patterns from phase differences. Near-zero path differences synchronize wavefronts across the beam, establishing a uniform phase—the null point, essential for data acquisition given the finite coherence length *L*, denoting the maximum path difference for which interference effects are observable. The coherence length of a gaussian source can be calculated by:

$$L = \frac{\lambda^2}{\pi} \frac{2\ln 2}{\Delta\lambda}, \tag{1}$$

where $\lambda$ is the central wavelength of the light, and $\Delta\lambda$ is the spectral width of the source. Prior to data acquisition, the coherence length can be estimated using Equation (1) to ensure a discernible interference pattern.

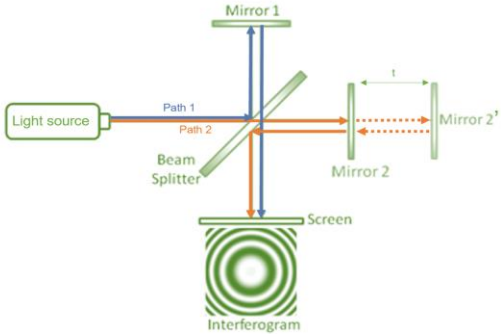


Fig.1. The setup of a Michelson interferometer, consisting of two mirrors and a beam splitter. The light source emits a beam that is divided by the beam splitter along two paths. In path 1, the beam reflects off the beam splitter and then from mirror 1. Path 2's beam transmits through the beam splitter and is reflected by the moveable mirror 2, enabling a variable path difference. A displacement t of mirror 2 results the path difference changing by 2t.

Adjusting mirror 2 in the Michelson interferometer allows for the capture of an interferogram, illustrating intensity variations of the resultant interference pattern due to path differences. Ensuring an appropriate mirror velocity is vital for data quality. Adhering to the Nyquist-Shannon theorem, complete signal representation requires a sampling rate over twice the signal's frequency [5]. Given a sampling rate of *p*, the maximum mirror speed v can be calculated by:

$$v = \frac{p\lambda}{2}, \tag{2}$$

where λ represents the central wavelength of the source.

Upon obtaining an interferogram expressed as *E(x)*, applying the Fourier Transform yields its power spectrum in the frequency domain, which enables the extraction of the light source's spectral distribution *E(k)* by applying:

$$E(k) = \mathcal{F}[E(x)]. \tag{3}$$

This can be recalculated to acquire a wavelength spectrum, *E(λ)*, utilizing the inverse proportionality between wavelength and frequency.

### B. Color characteristics of white light

#### 1) CIE color spaces

Retinal cells, utilizing three types of cone cells sensitive to red, green, or blue light, do not discern spectral power distribution [6]. This insight led the International Commission on Illumination (CIE) to experiment in the 1930s, demonstrating that any color could be mimicked by combining red, green, and blue light [7]. The experiment's outcomes, plotted as the amount of primary red, green, and blue light needed for each visible spectrum color, yielded the CIE standard observer color matching functions *x(λ), y(λ),* and *z(λ),* depicted in Fig. 2. We can further calculate the X, Y and Z values that indicate how much red, green and blue a color is made, by means of:

$$\begin{aligned} X &= \int_{380}^{780} X(\lambda)\ d\lambda = \int_{380}^{780} x(\lambda) * E(\lambda)\ d\lambda; \\ Y &= \int_{380}^{780} Y(\lambda)\, d\lambda = \int_{380}^{780} y(\lambda) * E(\lambda)\ d\lambda; \\ Z &= \int_{380}^{780} Z(\lambda)\ d\lambda = \int_{380}^{780} z(\lambda) * E(\lambda)\ d\lambda, \end{aligned} \tag{4}$$

where *X(λ), Y(λ)* and *Z(λ)* represent the distribution of the three colors in a given spectrum $E(\lambda)$. 380 and 780, in nm, is the minimum and maximum of wavelength of visible light that XYZ values are defined.

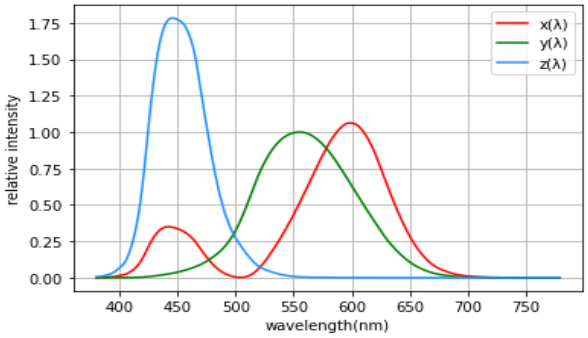


Fig.2. Plot of x(λ), y(λ), and z(λ), describing the variation in human eye sensitivity to red, green, and blue colors across different wavelengths. The peaks of these curves correspond to the wavelengths of red, green, and blue light, specifically at 595 nm, 563 nm, and 440 nm, respectively. Data come from CIE 1931 color spaces [8].

In a more intuitive way, XYZ can be converted to RGB values, indicating the proportions of standard red, green, and blue in an arbitrary color, enabling color reconstruction on computer screens. This can be done by matrix multiplication:

$$\begin{bmatrix} R \\ G \\ B \end{bmatrix} = \begin{bmatrix} 3.2404542 & -1.5371385 & -0.4985314 \\ -0.9692660 & 1.8760108 & 0.0415560 \\ 0.0556434 & -0.2040259 & 1.0572252 \end{bmatrix} \begin{bmatrix} X \\ Y \\ Z \end{bmatrix}, \quad (5)$$

where here XYZ should be normalized, scaling from 0 to 1.

*2) Correlated Color Temperature*

Correlated Color Temperature (CCT) describes the perceived warmness or coolness of white LED light, comparing its hue to a Planckian radiator's color at a specific temperature [9]. Measured in Kelvin (K), CCT doesn't indicate the light source's actual temperature but its color appearance. Lower CCT values (2000K-3000K) represent warm yellow hues, while high CCTs (above 5000K) yield cool blue tones. This counterintuitive aspect arises from the black body radiation curve shifting to shorter wavelengths at higher temperatures and longer wavelengths at lower temperatures. CCT can be calculated by:

$$CCT = 449n^3 + 3525n^2 + 6823.3n + 5520.33,$$
$$where\ n = \frac{X-0.3320(X+Y+Z)}{0.1858(X+Y+Z)-Y}. \quad (6)$$

This formula, derived from McCamy's approximation, asserts a maximum absolute error under 2 Kelvin for color temperatures between 2856 and 6500 K [10].

*3) Color Rendering Index*

Color Rendering Index (CRI) is a quantitative measure of a light source's ability to reveal the colors of various objects faithfully in comparison to a natural light source. Rated on a scale from 0 to 100, higher CRI values indicate better color rendering. This is particularly important in manufacturing white LEDs, as a higher CRI ensures that the light they emit allows objects to appear in their true colors, closely resembling how they would look under natural sunlight [11]. In spite CRI calculation is complicated, it can be streamlined using XYZ values to determine the corresponding CRI through a Python script provided by CIE [12].

## III. Method

Referring to Fig.1, we constructed a setup to measure white LED interference patterns, as depicted in Fig.3. A Helium-Neon Laser was incorporated as the light source, emitting highly monochromatic red light at 632.8 nm. This single-wavelength light aids in correcting instabilities in mirror movement, thereby stabilizing spacing of path difference.

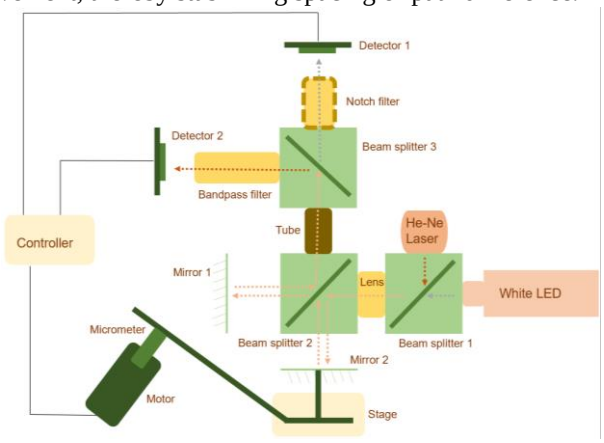


Fig.3. Illustration of our experimental setup. Light from a white LED and a He-Ne laser follows a common path to Beam Splitter 3. Only the laser's red light penetrates the Bandpass filter, reaching Detector 1. The Notch filter permits all but red light, enabling Detector 2 to primarily capture LED emissions. Both detectors link to a Controller, which also interfaces with a motor, manipulating Stage and Mirror 2 to induce path differences. A 25mm focal length lens is used to broaden the interference pattern.

### A. Movement of Moter

Mirror 2's movement is motor-driven, rotating Micrometer in μsteps, which translates to nm for stage and mirror displacement. A conversion factor of approximately 0.0156 nm/μstep, based on the apparatus's manufacturing parameters [13], is estimated. According to Equation (2) and with p=50 Hz and λ=780nm, the motor's maximum velocity for data reconstruction is calculated at 1250000 μsteps/s. However, through trial experiments, a velocity of 30000 μsteps/s was chosen to minimize background noise impact.

The coherence length of the white LED, manually measured at 21000±3500 nm, surpasses its theoretical value of 6800 mm calculated from Equation (1), possibly due to the LED's non-Gaussian nature. Based on trial experiments, the motor was set to move 4000000 μsteps (~60000 nm) each time in the measurements, optimizing interferogram clarity and reducing background noise.

### B. Crossing point analysis

In the interferometer, the recombination of He-Ne laser's monochromatic beams leads to stable fringe patterns from fixed-point interference, reflected in evenly spaced x-axis crossings of the interferogram, each equating to half the laser's wavelength (316.4 nm). Motor instability, however, results in irregular mirror movements per μstep, making these crossing points appear unevenly spaced, as shown in Fig.4.

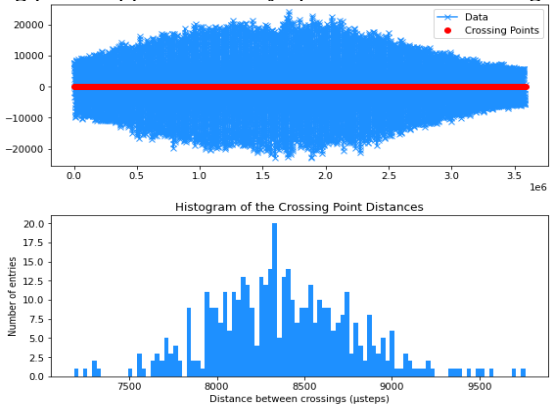


Fig.4. Initial interferogram and a histogram depicting distances between crossing points in the He-Ne laser interferogram. The graph's Gaussian-like distribution features a peak that aligns with the theoretical spacing.

The Gaussian nature of the histogram, in line with the Central Limit Theorem, implies motor instability. We counteract this by shifting the data points to equal spacing, 316.4nm. Utilizing cubic spline interpolation, we resample the white LED data to produce a corrected interferogram with uniformly spaced data points, as shown in Fig.5.

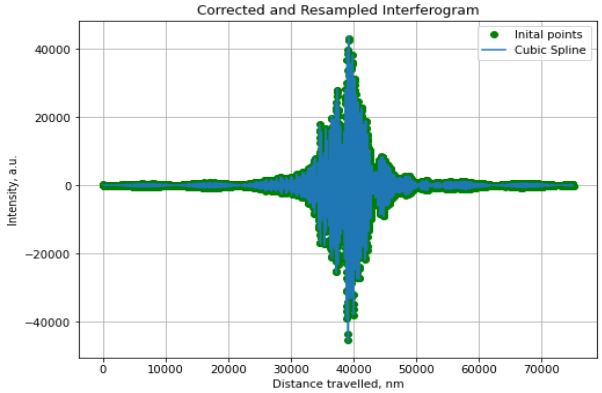


Fig.5. Initial white LED interferogram data points (green) are depicted alongside 3000000 resampled points using cubic spline (blue). Subsequent analyses will be based on this resampled dataset.

### C. *Bandpass filter and Notch filter*

In our experiment, we employed a Bandpass filter transmitting light at 633±5 nm [14], ensuring detection of He-Ne laser light by Detector 1 for its interferogram acquisition. The use of a Notch filter, transmitting all but 633±25 nm wavelengths [15], was debated. It effectively blocks laser light but also red light from the LED, as Fig.6(a) illustrates. Without the Notch filter, differentiation between laser and LED light is challenging, as shown in Fig.6(b) Measurements were conducted under both scenarios, and the resulting interferograms were analyzed to inform our decision-making.

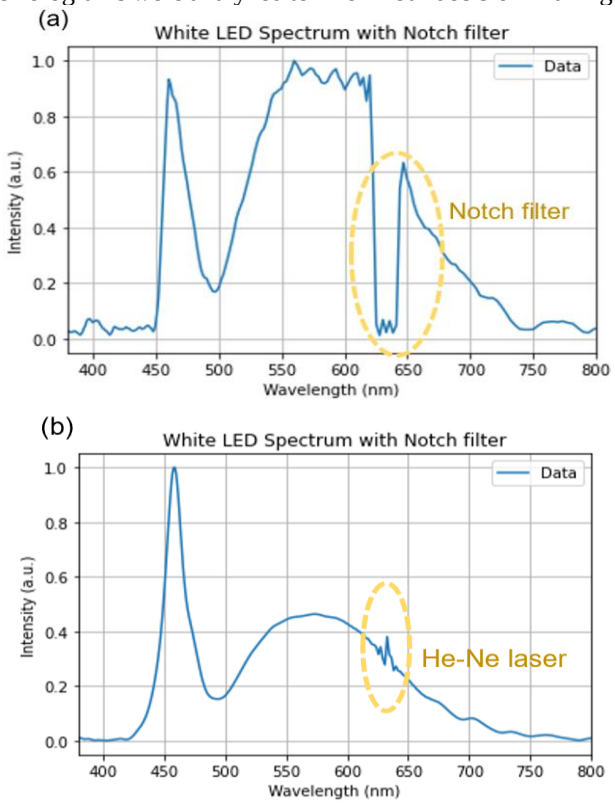


Fig.6. Spectral analysis of a white LED, post Fourier Transform of its interferogram, compares scenarios with and without a Notch filter. Utilizing the Notch filter significantly attenuates the LED's red component, nearly to zero. In contrast, without the filter, a distinct hump corresponding to the He-Ne laser's red light is evident. Notably, the spectrum obtained with the Notch filter exhibits increased noise.

The influence of the He-Ne laser on the spectrum is minimal, indicated by a small hump likely from the laser's dim emission. Given the necessity of extracting the red component in subsequent analyses without losing its red characteristics, we opted against using the Notch filter. Additionally, Python-based linear interpolation can remove this hump, yielding a smoother spectrum. The resulting flattened spectrum is presented in Fig.7.

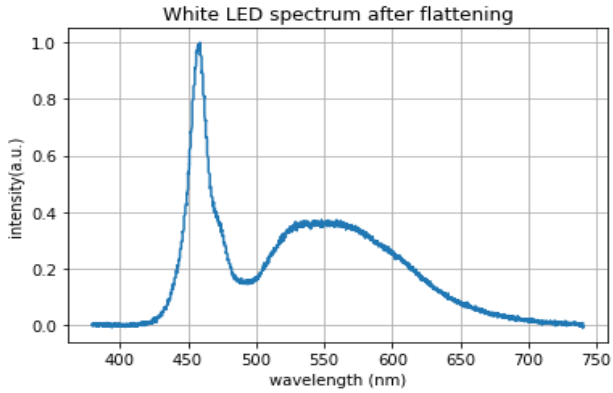


Fig.7. Flattened spectrum of white LED, post-removal of the He-Ne laser-induced hump. This adjusted spectrum represents our predicted 'real' spectrum of the white LED, serving as the basis for subsequent analyses.

## IV. Results and Discussions

### A. *Lighting principle of white LEDs*

LED chips emit within a 10–25 nm range, differing from broad-spectrum radiators like daylight and filament lights [16]. For white light, LED spectra are often merged or modified. Commonly, blue "pump" LEDs are used, with yttrium aluminum garnet (YAG) with cerium (Ce) phosphors converting light to longer wavelengths [17]. To verify if our experiment's white LED follows this method, we substituted it with a lab-provided blue LED and measured its interferogram. The spectra of both LEDs are shown in Fig.8.

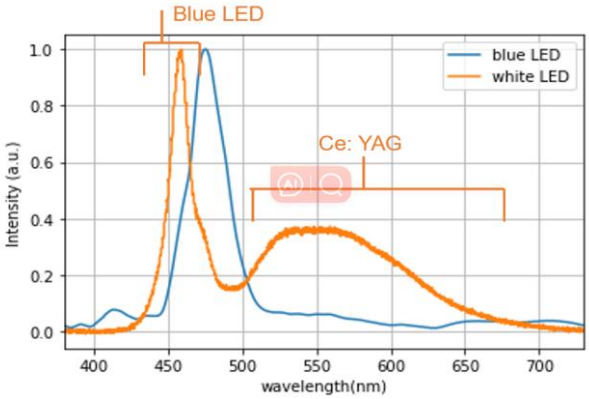


Fig.8. The spectra of both white and blue LEDs exhibit peaks in the blue region, at 457.7 nm for white and 468.5 nm for blue. The white LED spectrum also shows a smoother peak at 552.5 nm, suggesting reemission of green and red light by Ce:YAG phosphor.

The spectrum indicates that the white LED indeed utilizes phosphor for white light emission. However, the first peak of the white LED spectrum does not align perfectly with the peak of blue LED spectrum. This discrepancy could arise from manufacturing variations, where the blue LED within the white LED differs from the lab-provided blue LED, despite sharing the same manufacturer. Alternatively, it may stem from the phosphor's reemission properties, warranting further investigation.

### B. *Color analysis of the white light*

The white LED's phosphor emits green and red light, combining with blue LED emissions for white light production. Using Equation (4), the spectrum in Fig.1 was multiplied by the white LED's spectral data, resulting in X(λ), Y(λ), and Z(λ). These values represent the red, green, and blue distribution in the LED's spectrum E(λ), as depicted in Fig.9. Numerical integration via the trapezoidal rule calculated X, Y, and Z values as 21.48±0.03, 22.06±0.04, and 20.22±0.02, respectively, with uncertainties attributed to integration inaccuracies and computed using Python. Notably, the LED emits more red light and green light than blue light, potentially indicating a relatively warm light emission. Equation (5) was applied to determine the LED's emitted RGB values as (255.00±0.13, 250.47±0.22, 240.95±0.08), with uncertainties derived from an uncertainty propagation function:

$$F = f(X, Y, Z,)$$

$$\sigma_F = \sqrt{(\frac{\partial f}{\partial X})^2\sigma^2 X + (\frac{\partial f}{\partial Y})^2\sigma^2 Y + (\frac{\partial f}{\partial Z})^2\sigma^2 Z}, \qquad (7)$$

where F represents the function associated to R, G, B values.

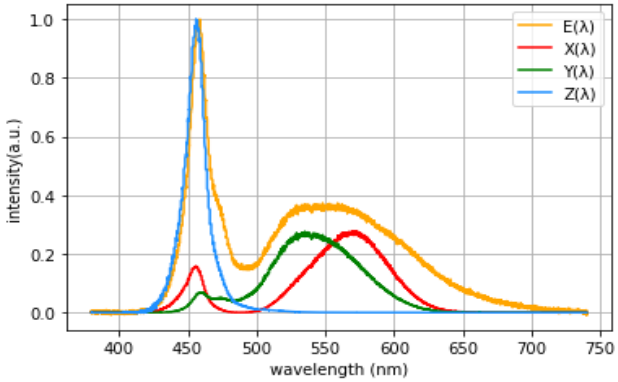


Fig.9. Red, green, and blue components are identified in the white LED spectrum. The blue component closely aligns with the white LED spectrum's first peak, reflecting the blue LED's light emission. The white LED spectrum's second peak reveals emissions of both red and green lights.

The color composition of the white LED is contrasted with the ASTM E-490 AM0 Standard Solar Spectra (Sunlight) [18]. The red, green, and blue components were computed similarly, as depicted in Fig.10.

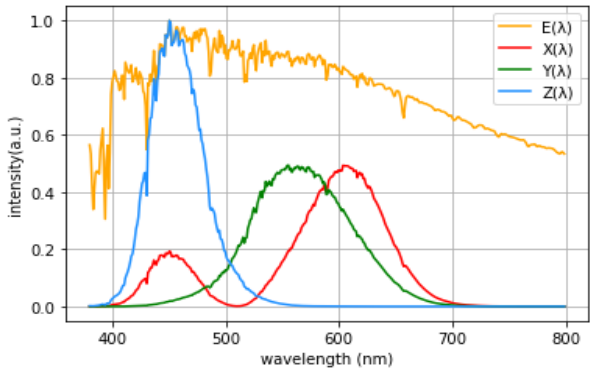


Fig.10. The sunlight spectrum's red, green, and blue components are analyzed. Compared to the white LED, sunlight exhibits a more uniform distribution across the visible wavelength range, resulting in a more balanced color distribution.

XYZ and RGB values for sunlight are calculated as (51.92±0.05, 53.55±0.04, 56.26±0.07) and (217.19±0.53, 234.42±0.74, 255.00±0.32), respectively. Relative to sunlight, the white LED exhibits more red and green but less blue. Utilizing their RGB values, colors of both sunlight and the white LED are reconstructed on a computer screen, as presented in Fig.11.


Fig.11. Colors of sunlight and the white LED, derived from our calculations, are displayed. Contrary to intuition, the sunlight appears 'cooler' than the white LED.

CCT values for sunlight and the white LED, calculated using Equation (6), are 5702±15K and 5129±23K, respectively. The higher CCT of sunlight indicates more short-wavelength emission, appearing 'cooler,' aligning with our color reconstruction in Fig.11. Sunlight's theoretical CCT is around 5900K, only 3.4% differ from our calculated value, suggesting the high reliability of both the white LED's CCT and our color reconstruction.

The CRI value of the white LED is calculated at 68, without associated uncertainty. This is due to the Python program's discrete level computation, precluding uncertainty propagation application in Equation (7). This CRI is typical for LEDs, suggesting they can reasonably reproduce object colors under their illumination, akin to natural light conditions. Sunlight, an ideal Planckian radiator, has a CRI of 100. For a more comprehensive understanding of CRI, comparing LEDs with different CRI values would elucidate to what extent they can accurately reproduce object colors.

## V. Conclusion

In our experiment, a Michelson interferometer provided a white LED's interferogram, Fourier transformed to its power spectrum. By comparing with a blue LED's spectrum, we confirmed the white LED's emission of blue light, followed by red and green light reemission from the phosphor. We quantified the red and green reemissions and reconstructed the LED's color using calculated RGB values. Comparing with sunlight, an ideal Planckian radiator, we found the white LED's Correlated Color Temperature to be 5129±23K, indicating warmer emission than sunlight. The Color Rendering Index was determined to be 68, which reflects the moderate ability of the white LED to render objects' colors.

Several aspects of the experiment merit evaluation. The bandpass filter transmitted both He-Ne laser light and the LED's red component, suggesting crossing point spacing variations might result from white LED's incoherent red light, not just motor inconsistency. Consequently, interferogram correction may be questionable. Additionally, linear interpolation removed the spectrum's hump without the Notch filter, but a more refined method, like subtracting the He-Ne laser spectrum, might be more accurate, though determining the correct intensity subtraction is challenging. Involving the He-Ne laser, while helpful, introduced some complexities.

Future investigations could explore disparities between the white and blue LED spectra, potentially attributable to phosphor reemission properties. Studying phosphor materials could yield further insights. Sunlight variability across locations and conditions suggests analyzing more data sets for diverse CCT results. Experimenting with white LEDs of different CCTs and CRIs could enhance understanding of phosphor behavior in varying light conditions.

## REFERENCES


[1] Albert Michelson; Edward Morley (1887). "On the Relative Motion of the Earth and the Luminiferous Ether". American Journal of Science. 34 (203): 333–345.

[2] R. Comerford, “Led specs - understanding the color white,” DigiKey, https://www.digikey.co.uk/en/articles/led-specs---understanding-the-color-white (accessed Dec. 13, 2023).

[3] A. E. Roggio, “Creating white light by adding - not subtracting - color,” DigiKey, https://www.digikey.co.uk/en/articles/creating-white-light-by-adding---not-subtracting---color (accessed Dec. 13, 2023).

[4] S. Keeping, “Whiter, brighter leds,” DigiKey, https://www.digikey.co.uk/en/articles/whiter-brighter-leds (accessed Dec. 13, 2023).

[5] Marks, II, R.J., ed. (1993). Advanced Topics in Shannon Sampling and Interpolation Theory (PDF). Springer Texts in Electrical Engineering. Springer. doi:10.1007/978-1-4613-9757-1. ISBN 978-1-4613-9757-1.

[6] S. Keeping, “Defining the color characteristics of white leds,” DigiKey, https://www.digikey.co.uk/en/articles/defining-the-color-characteristics-of-white-leds#:~:text=Manufacturers%20produce%20white%20LEDs%20with,batch%20have%20slightly%20different%20spectra. (accessed Dec. 13, 2023).

[7] A. David and L. A. Whitehead, “LED-based White Light,” Comptes Rendus Physique, vol. 19, no. 3, pp. 169–181, 2018. doi:10.1016/j.crhy.2018.02.004

[8] CIE (1932). Commission internationale de l'Eclairage proceedings, 1931. Cambridge: Cambridge University Press.

[9] M. Pharr and G. Humphreys, Physically Based Rendering: From Theory to Implementation. Amsterdam etc.: Elsevier, 2004.

[10] R. McCluney, Introduction to Radiometry and Photometry. Boston: Artech House, 2014.

[11] “Introduction to Light, Color and Color Space,” Introduction to light, color and color space, https://www.scratchapixel.com/lessons/digital-imaging/colors/color-space.html (accessed Dec. 13, 2023).

[12] “ColorTools: Tools for spectral analysis,” Interface Innovations :: Colortools, https://interfaceinnovations.org/colortools.html (accessed Dec. 13, 2023).

[13] H. Crespo, “Interferometry,” Advanced Practical Physics Year 2 Teaching Labs, pp. 30–31, Nov. 2023.

[14] “Hard-coated UV/VIS bandpass filters,” Thorlabs, Inc. - Your Source for Fiber Optics, Laser Diodes, Optical Instrumentation and Polarization Measurement & Control, https://www.thorlabs.com/newgrouppage9.cfm?objectgroup_id=1860&pn=FLH633-5 (accessed Dec. 13, 2023).

[15] “Notch filters,” Thorlabs, Inc. - Your Source for Fiber Optics, Laser Diodes, Optical Instrumentation and Polarization Measurement & Control, https://www.thorlabs.com/newgrouppage9.cfm?objectgroup_id=3880&pn=NF633-25 (accessed Dec. 13, 2023).

[16] THE SIMPLE METHOD OF THE RGB TO SPECTRUM CONVERSION FOR TASKS OF PHYSICALLY BASED RENDERING, https://sv-journal.org/2015-4/03/en/index.php?lang=en (accessed Dec. 13, 2023).

[17] A. C. Berends, M. A. van de Haar, and M. R. Krames, “YAG:CE3+ phosphor: From micron-sized workhorse for general lighting to a bright future on the nanoscale,” Chemical Reviews, vol. 120, no. 24, pp. 13461–13479, 2020. doi:10.1021/acs.chemrev.0c00618

[18] “SSI reference spectra,” NASA, https://sunclimate.gsfc.nasa.gov/ssi-reference-spectra (accessed Dec. 13, 2023).